N84-26554

NASA

Technical Memorandum 86120

COALESCENCE OF TWO PRESSURE WAVES ASSOCIATED WITH STREAM INTERACTIONS

Y. C. Whang
L. F. Burlaga

APRIL 1984

National Aeronautics and
Space Administration

Goddard Space Flight Center
Greenbelt, Maryland 20771

COALESCENCE OF TWO PRESSURE WAVES ASSOCIATED WITH STREAM INTERACTIONS

Y. C. Whang
Department of Mechanical Engineering
Catholic University of America
Washington, D.C. 20064

L. F. Burlaga
Laboratory for Extraterrestrial Physics
NASA - Goddard Space Flight Center
Greenbelt, MD 20771

Short Title: Collision of Shocks

April, 1984

ABSTRACT

An MHD unsteady 1-D model is used to simulate the interaction and coalescence of two pressure waves in the outer heliosphere. Each of the two pressure waves was a compression region bounded by a shock pair. Computer simulation using Voyager data as input demonstates the interaction and coalescence process involving one pressure wave associated with a fast stream and the other pressure wave without a fast stream. The process produced a significant change in the magnetic field and plasma signatures. The propagation of the forward and reverse shocks first widened the radial dimension of the shock compression region with increasing heliocentric distances. The shocks belonging to two neighboring compression regions eventually collided and the two compression regions began to overlap with each other. Both shocks continued to propagate after the collision but they were weakened. As a result of the collision, a contact surface formed in the second generation compression region bounded by the two shocks. The second shock compression further enhanced the magnetic field, plasma density and temperature in the new compression region. This type of interaction is a dominant dynamical process in the outer heliosphere, and it can significantly and irreversibly alter the structure of the medium.

1. INTRODUCTION

Numerical simulations for the development of shock pairs have been studied using two approaches: the unsteady 1-D models, and the quasi-steady corotating models. The former has been used to study the gasdynamic evolution of stream structures (Hundhausen, 1973a,b; Hundhausen and Gosling,1976; and Gosling et al.,1976) and the MHD simulation of interplanetary shock pairs (Steinolfson et al.,1975; Dryer and Steinolfson,1976; and Dryer et al.,1978; Whang, 1984). The latter has been used to study MHD formation of shocks in corotating stream structures (Whang and Chien, 1981; Pizzo, 1982; and Burlaga et al., 1984).

Solar wind observations made by Pioneer 10 and 11 confirmed the predictions that the shock pairs which form in front of corotating high-speed streams should be prominent features of the large-scale solar wind structure near 5 AU (Dessler and Fejer, 1963; and Hundhausen, 1973b). Hundhausen and Gosling (1976) found that the solar wind speed observed by Pioneer 10 beyond 4 AU revealed a prevalent sawtooth-like profile. Their calculation shows that the evolution of a stream between 1 AU and 6 AU leads to the formation of a forward-reverse shock pair. At 4 AU the pair exhibits a double-sawtooth volocity profile similar to that observed by Pioneer 10. The calculation also shows a large enhancement in plasma density in the compression region bounded by the shock pair. An independent analysis of Pioneer 10 and 11 magnetic field and plasma observations by Smith and Wolfe (1976) reported the observation of large enhancements in density, temperature, field strength, and fluctuation level in the regions bounded by the shock pairs. This observation has strengthened the

interpretation regarding the existence of shock pairs in the solar wind stream structure beyond 1 AU.

To include the magnetic field effects in the simulation model, Dryer and Steinolfson (1976) computed the evolution of two forward-reverse MHD shock pairs between 0.3 and 10 AU from simulated twin coronal hole streams. Recently Whang (1984) introduced a new approach to study the development of the forward-reverse MHD shock pair at large heliocentric distances using an MHD unsteady 1-D model. The method which treats each shock as a surface of discontinuity of zero thickness becomes particularly effective in the region where the interaction of discontinuity surfaces (such as collision or merging of shocks) take place. The forward and reverse shocks which form at the leading edge and propagate in opposite directions continues to widen the radial dimension of the shock compression region (pressure wave). The shock compression region evolves with increasing heliocentric distances to become an increasingly important large-scale dynamical structure of the interplanetary medium at large heliocentric distances. The total pressure, the magnetic field and plasma density in the shock compression region are significantly greater than those outside its shock boundaries.

Theoretical treatment of quasi-steady hydrodynamic corotational interplanetary structures were first introduced by Carovillano and Siscoe (1969), and Siscoe and Finley (1972). Pizzo (1978,1980) numerically simulated the evolution of corotating streams. Whang (1980) theorized that the MHD process of a corotating interplanetary structure consists of the

expansion of the solar wind in streamtubes and the MHD interaction between neighboring streamtubes. The method of characteristics has been introduced to study the interaction process. Whang and Chien (1981) studied the formation of MHD shocks at the leading edge of corotating streams in region between 0.5 AU and 1.3 AU. Their solutions show that near 1 AU a shock pair may form only when the initial leading edge region of a corotating stream is sufficiently narrow and that corotating shocks do not necessarily occur there in pairs. A corotating reverse shock can form without a forward shock nearby, as in the obvervation reported by Burlaga (1970). Pizzo (1982) used a 3-D MHD model to simulate the three dimensional evolution of a corotating structure associated with interplanetary flow issuing from an isolated equatorial coronal hole. His result predicted that both forward and reverse shocks form nearest the sun along the equator and gradually move to higher latitudes. The reverse shock appears first, being readily discernable by 0.5 AU over a small range of latitudes about the equator. The forward shock forms somewhat later but over a much wider arc. His predicted shocks appear to occur much closer to the sun than is generally observed.

The solar wind inside and near 1 AU is dominated by numerous small streams, transient flows and shocks, and a few large corotating streams. These structures are closely related to the conditions in the corona and carry strong identifiable signatures of their solar origins. At large heliocentric distances, large corotating streams sweep up the slower transient and/or corotating streams, pressure waves and shocks. They coalesce to

form large-scale new structures dominated by pressure waves. At large heliocentric distances, these large-scale structures remain identifiable even when other stream structures become invisible. This evolution process has been presented by Gosling et al. (1976), Burlaga et al.(1983), Burlaga (1983), and Burlaga and Goldstein (1984). Dryer and Steinolfson (1976) and Dryer et al.(1978) have calculated the collision between the forward and reverse shocks from adjacent shock pairs associated with two identical corotating streams. Burlaga (1983) and Pizzo (1983) estimated that at 20-25 AU shocks from successive Carrington rotations have had time to propagate all the way across the intervening structures and meet. Thus, at those distances the entire flow should have been shocked at least once if it were quasi-stationary. Shock compression regions should eventually become the dominant large-scale structures of the interplanetary medium in the outer heliosphere.

The shock interaction processes which dominate the large scale variations of the distant solar wind may include three basic elements: (a) interaction of a shock with the stream structure or contact surfaces, (b) collision of a forward and a reverse shock, and (c) merging of two forward or two reverse shocks. This paper attempts to study the shock collision problem using Whang's MHD unsteady 1-D model.

2. NUMERICAL TECHNIQUES

Two major numerical techniques have been used for the calculation of MHD shocks in the heliosphere : finite-difference methods and the method of characteristics. They both calculate the flowfield properties at discrete grid points but the two construct the numerical grid very differently. Also there are two numerical methods to describe a shock at large heliocentric distances: a discontinuous description and a numerically smeared description. This paper treat shocks as surfaces of discontinuity with zero thickness. In many previous studies of shocks in the heliosphere, shocks are described as regions of large gradients spread over several grid points. Some of the numerically smeared descriptions of shocks using finite-difference technique introduce an artificial diffusivity to provide a mathematical dissipation analogous to the real diffusion effects inside a shock wave.

Our method uses the shock surfaces to divide the domain of solutions into several flow regions. The jump conditions of MHD shocks describe the flow conditions across the boundaries between flow regions and the method of characteristics describes the variation of flow conditions in each region. At grid points on the shock boundary each flow variable has two values - the condition on the front and on the back side of the shock. This method can calculate the variations in shock speeds and shock strength more accurately.

Our method becomes particularly useful for the study of shocks interaction (collision or merging) in the outer heliosphere, because this method can sharpen its focus at the

detailed dynamical structures in the region where the action takes place. For shock interaction problems, two or more discontinuity surfaces are present near the interaction point at a given time. The method of characteristics allows a flexible adjustment of the grid sizes in the flow region between two neighboring discontinuity points. Thus, one can maintain a reasonable number of grid points between two discontinuity points for a meaningful description of the flowfield. One can also adjust the time interval Δt compatible with the physical distance between two closest discontinuity points. The solutions calculated by this technique would not smear out any important features resulting from shock interaction. The merging of two forward or reverse shocks produces a stronger shock and a contact surface on its back side. The merging process contributes to the evolution of complicated corotating structures into simpler large-scale structures. The present paper uses this method of solutions to study the collision of a forward and a reverse shock.

We use a simple unsteady 1-D model to study the formation and interactions of MHD shocks at large heliocentric distances. In a heliocentric spherical coordinates system (r, θ, ω), the model assumes that (a) the flow properties near the equatorial plane ($\theta = \pi/2$) are function of r and t only, and (b) the flow velocity

$$\vec{u} = u \vec{e}_r$$

and the magnetic field

$$\vec{B} = B \vec{e}_\omega .$$

In each continuous flow region, the flow conditions are governed by a system of four equations:

$$\frac{d}{dt}\left(p\,\rho^{-5/3}\right) = 0 \tag{1}$$

$$\frac{d}{dt}\left(\frac{B}{r\rho}\right) = 0 \tag{2}$$

where $\frac{d}{dt} = \frac{\partial}{\partial t} + u\frac{\partial}{\partial r}$ represents the time derivative following the motion of each fluid element, and the two characteristic equations

$$\left(\frac{\partial p^*}{\partial t}\right)_{\pm} \pm \rho\, C_f \left(\frac{\partial u}{\partial t}\right)_{\pm} = s_{\pm} \tag{3}$$

where $\left(\frac{\partial}{\partial t}\right)_{\pm} = \frac{\partial}{\partial t} + (u \pm C_f)\frac{\partial}{\partial r}$

and $s_{\pm} = \frac{\rho}{r}\left[a^2(u \mp C_f) \mp C_f \frac{GM}{r} - 2uC_f^2\right]$

In the above equations, p is the thermal pressure, ρ the plasma density, p* the total pressure (sum of the thermal and the magnetic pressure), a the Alfven speed, c the gasdynamic sound speed, $C_f = (c^2 + a^2)^{1/2}$ the fast speed, G the gravitational constant, and M the mass of the sun. A detailed discussion of these equations and the method of numerical integration can be found in Whang (1984).

3. INITIAL CONDITIONS

The initial conditions for this study are generated from the two shock pairs observed by Voyager 2 in October 1978 (Figure 1). The data points are hourly averages of the plasma and magnetic field. Let the two shock pairs be identified as Pair A and Pair B. The four shocks are respectively identified as FA, RA, FB, and RB (F for forward shock and R for reverse shock). The plasma and field outside of the shock pairs are in an unshocked state. The shock compression regions bounded by the shock pairs are two pressure waves. The total pressure, magnetic field and plasma density in the shock compression region are significantly greater than those outside its shock boundaries. The two shock pairs are initially unequal in strengths: Pair A is much stronger than Pair B. We study the interaction and coalescence of the two pressure waves. Smooth curves which represent the data points are used as the initial condition for numerical simulation of the prosess. The curve fitting procedure was carried out in the logarithmic scale plots for the field magnitude, the number density, and the total pressure, in linear scale plots for the velocity.

The shock pair A observed by Voyager 2 near 4.07 AU consists of fully-developed shocks. The flow velocity exhibits a flat profile in the shock compression region enclosed by the shock pair. The flat profile and the small separation between FA and RA indicate that the shock pair formed at the leading edge region of a large stream just began to propagate in the rarefaction regions of the stream structures.

The formation of the shock pair B, which was observed by Voyager 2 near 4.02 AU, must have been completed several days

before the formation of Pair A. The separation between FB and RB is much greater than that of Pair A. The shocks were moving apart into rarefaction regions on either side (see p^* in Figure 1). As the reverse shock RB moved into a rarefaction region, the flow speed behind RB decreased nearly at the same pace as the speed on the front side. Similarly, the speed behind the FB increased as the shock propagated. As a result, a visible slope in velocity profile was generated in the shock compression region to form the double-sawtooth configuration at the orbit of Voyager 2.

The two shock pairs (A and B) have been observed by both Voyager 1 and 2 (Figure 2). As Voyager 2 data are used as input, the initial state of the four shocks (shock speeds and shock strengths) have to be carefully adjusted so that the plasma and field calculated at the Voyager 1 orbit are in good agreement with observation. The two spacecraft observed a significant increase in separation between two shocks for each pair. The propagation of the shocks continued to widen the radial dimension of the shock compression region. The two pressure waves eventually coalesced.

4. COLLISION OF A FORWARD AND A REVERSE SHOCK

The collision of two shocks FA and RB demonstrates the principal result of the coalescence of two pressure waves. The numerical solutions show that a second-generation shock compression region bounded by RB and FA was produced after the collision of the two shocks as shown in Figure 3. A contact surface (CS) appeared in the new compression region. Figure 4 plots the variation of the state of each shock wave represented by two parameters - the shock speed and the density ratio. The shock pair A driven by a large stream continued to grow in shock strength in days 0 to 3. The two shocks FA and RB collided on day 6.8. Both FA and RB were weakened as a result of the collision. The top panel of Figure 4 shows the variation of the shock speeds during the 20 days period and the sudden change in shock speeds due to collision. Those who are interested in the gradual evolution of the shock pair may find useful information from a printout of several shock parameters in Table 1. The first three columns identify the time, heliocentric distance, and the pre-shock flow speed; other columns identify the shock speed, various parameters measuring the shock strength, and flow conditions in front of the shocks.

Figure 5 shows the evolution of the flow speed. When the shock pair interacted with the rarefaction regions, the flow conditions of the rarefaction region in front of each shock were not perturbed by the approaching shock. The jump in flow speed increased as the strength of the shock FA continued to grow from day 0 to day 4. This caused an increase in flow speed behind FA as the shock propagated forward. During the first four days, the

shock RB grew in strength as it propagated into a rarefaction region. The flow speed behind the reverse shock RA decreased more rapidly than the speed on the front side. As a result of this interaction, visible positive slopes in u,r-profiles are generated in the shock compression region B on day 4. After day 6.8, the flow speed remained continuous across the contact surface in the second-generation shock compression region. As FA moved into a region with increasing flow speed and RB moved into a region with decreasing flow speed, the flow speed in the second-generation shock compression region again evolved from a flat profile to a positive slope. The flow speeds eventually evolved into another sawtooth configuration on day 20.

The total pressure is plotted in Figure 6 and two distinct pressure waves (shock compression regions) are seen on day 0 at the bottom panel of the figure. After the collision of FA and RB, the profile of the total pressure changed significantly. Instead of two separate compression waves, one sees a single broad compression wave (see the top panel of Figure 6) with three component regions: a singly shocked region between RA and RB; a doubly shocked region between RB and FA; and a singly shocked region between FA and FB. The total pressure in the second-generation shock compression region is two orders of magnitude greater than that predicted by an adiabatic solar wind under the assumption that there were no shocks in the heliosphere. The heliospheric structure is reorganized as a result of the coalescence of two pressure waves.

Figures 7-9 show that the number density, the temperature

and the field magnitude are discontinuous across a contact surface that has formed as a result of the collision between FA and RB. The shock compression region A on day 4 had a minimun in the temperature profile. Because a conversion of kinetic energy into thermal energy takes place at shock crossings, the increases in temperature for a shocked plasma are considerably greater than those for an unshocked plasma which is compressed adiabatically through the same density ratio. The fluid elements at low temperature were initially located near the middle of the leading edge region prior to day 0. Their temperature changes were largely governed by the adiabatic compression process. On the two sides of the low temperature plasma, the fluid elements carried the memory of large changes in temperature which they experienced at shock crossings. This explains the highly nonuniform distributions of T in the shock compression region. The two shock pairs observed by Voyagers on October 1978 are not equal in shock strength. Pair A was much stronger than Pair B. Before the collision of FA and RB, the temperature jump across FA was much stronger than that across RB. The fluid elements which experienced a larger temperature increase across FA before collision stay on the left side of CS in Figures 7-9. Therefore, the temperature and the thermal pressure on the left-hand-side of CS are greater than those on the right-hand-side of CS. The balance of the total pressure across CS requires that the compression in magnetic pressure and plasma density must be lower on the left side of CS in order to compensate for the higher T on the left of CS. Thus in the second-generation shock compression region the temperature is higher and the field

magnitude and plasma density are lower on the side of the stronger initial shock pair.

ACKNOWLEDGEMENTS

We are grateful to Drs. H. Bridge and A. Lazarus for allowing us to use their plasma data from Voyager 1 and 2, to Dr. N. Ness for magnetic field data from Voyager 1 and 2. One of the us (YCW) was supported by the Atmospheric Sciences Section of the National Science Foundation under grant ATM-8119302 and by the National Aeronautics and Space Administration under grant NAGW-579.

REFERENCES

Burlaga, L.F., A reverse hydromagnetic shock in the solar wind, Cosmic Electrodynamics, 1,233,1970.

Burlaga, L.F., Corotating pressure waves without fast streams in the solar wind, J. Geophys. Res., 88, 6085, 1983.

Burlaga, L.F., and M.L. Goldstein, Radial variations of larre-scale magnetohydrodynamic fluctuations in the solar wind, submitted to J. Geophys. Res., 1984.

Burlaga, L.F., R. Schwenn and H. Rosenbauer, Dynamical evolution of interplanetary magnetic fields and flows between 0.3 AU and 8.5 AU: Entrainment, Geophys. Res. Lett., 10, 413, 1983.

Burlaga, L., V. Pizzo, A. Lazarus, and P. Gazis, Stream dynamics between 1 AU and 2 AU: a detailed comparison of observations and theory, submitted to J. Geophys. Res., 1984.

Carovillano, R.L., and G.L. Siscoe, Corotating structures in the solar wind,Solar Phys.,8,401,1969.

Dessler, A.J., and J. A. Fejer, Interpretation of Kp index and M-region geomagnetic storms, Planet. Space Sci., 11, 505,1963.

Dryer, M., and R.S. Steinolfson, MHD solution of interplanetary disturbances generated by simulated velocity perturbations, J. Geophys. Res., 81, 5413, 1976.

Dryer, M., Z.K. Smith, E.J. Smith, J.D. Mihalov, J.H. Wolfe, R.S. Steinnofson, and S.T. Wu, Dynamic MHD modelling of solar wind corotating stream interaction regions observed by Pioneer 10 and 11, J. Geophys. Res., 83, 4347,1978.

Gosling, J.T., A.J. Hundhausen, and S.J. Bame, Solar wind stream evolution at large heliocentric distances, J. Geophys. Res., 81, 2111, 1976.

Hundhausen, A.J., Nonlinear model of high-speed solar wind streams, J. Geophys. Res., 78, 1528, 1973a.

Hundhausen, A.J., Evolution of Large-scale solar wind structures beyond 1 AU, J. Geophys. Res., 78, 2035, 1973b.

Hundhausen, A.J., and J.T. Gosling, Solar wind structures at large heliocentric distances: An interpretation of Pioneer 10 observations, J. Geophys. Res., 81, 1436, 1976.

Pizzo, V.J., A three-dimensional model of corotating streams in the solar wind, 1, Theoretical foundations, J. Geophys. Res., 83, 5563, 1978.

Pizzo, V.J., A three-dimensional model of corotating streams in the solar wind, 2, Hydrodynamic streams, J. Geophys. Res., 85, 727, 1980.

Pizzo, V.J., A three-dimensional model of corotating streams in the solar wind, 3, Magnetohydrodynamic streams, J. Geophys. Res., 87, 4374, 1982.

Pizzo, V.J., Quasi-steady solar wind dynamics, in Solar Wind Five, edted by M. Neugebaur, NASA CP-2280, pp. 675-691, 1983.

Siscoe, G.L., and L.T. Finley, Solar wind structure determined by corotating coronal inhomogeneities, J. Geophy. Res.,77, 35,1972.

Smith, E.J., and J.H. Wolfe, Observations of interaction regions and corotating shocks between one and five AU: Pioneer 10 and 11, Geophys. Res. Lett., 3, 137, 1976.

Steinolfson, R.S., M. Dryer, and Y. Nakagawa, Numerical MHD simulation of interplanetary shock pairs, J. Geophys. Res., 80, 1223, 1975.

Whang, Y.C., A magnetohydrodynamic model for corotating interplanetary structures, J. Geophys. Res., 85, 2285, 1980.

Whang, Y.C., The forward-reverse shock pair at large heliocentric distances, submitted to J. Geophys. Res., 1984.

Whang, Y.C., and T.H. Chien, Magnetohydrodynamic interaction of solar wind streams, J. Geophys. Res., 86, 3263-3272, 1981.

Table 1a Variation of shock parameters for RA and FA

day	AU	u_1 km/s	S km/s	p_2^*/p_1^*	n_2/n_1	$\lvert u_1-u_2\rvert$ km/s	C_{f1} km/s	M_1	β_1
				REVERSE SHOCK RA					
0	3.62	639	447	9.0	2.64	119.0	73.1	2.62	0.631
1	3.88	627	433	8.3	2.56	118.2	77.1	2.51	0.549
2	4.12	610	419	8.8	2.61	117.9	73.6	2.59	0.518
3	4.36	592	399	10.9	2.77	123.4	67.5	2.86	0.501
4	4.58	576	375	14.8	2.99	134.0	60.9	3.31	0.483
5	4.80	562	369	16.9	3.07	130.6	54.8	3.53	0.457
6	5.01	551	366	18.7	3.13	125.6	49.9	3.70	0.421
7	5.22	541	363	20.4	3.18	121.6	46.1	3.85	0.377
8	5.43	533	361	21.9	3.21	118.6	43.3	3.98	0.330
9	5.64	526	358	22.8	3.23	115.7	41.4	4.05	0.281
10	5.84	520	355	23.1	3.23	113.3	40.3	4.07	0.235
11	6.05	515	353	22.9	3.22	111.8	40.1	4.04	0.193
12	6.25	511	349	22.2	3.19	111.4	40.9	3.97	0.155
13	6.45	508	344	21.1	3.16	112.4	42.6	3.87	0.122
14	6.65	506	338	19.6	3.11	114.0	45.1	3.72	0.095
15	6.84	505	333	17.9	3.05	115.1	48.1	3.56	0.074
16	7.03	503	329	16.3	2.99	115.1	50.7	3.41	0.059
17	7.22	500	327	15.1	2.93	114.1	52.8	3.28	0.049
18	7.41	497	326	14.1	2.88	111.8	53.8	3.18	0.043
19	7.60	495	328	13.4	2.85	108.3	53.8	3.10	0.040
20	7.79	492	332	13.0	2.83	103.5	52.4	3.06	0.040
				FORWARD SHOCK FA					
0	3.95	364	530	15.8	3.00	111.0	49.1	3.39	0.241
1	4.26	378	565	44.6	3.56	134.1	33.0	5.64	0.396
2	4.60	384	594	132.9	3.85	155.6	21.3	9.87	1.054
3	4.95	384	620	299.0	3.94	175.9	15.6	15.10	2.966
4	5.31	383	630	453.9	3.96	184.2	13.2	18.73	4.580
5	5.67	384	619	479.0	3.96	175.8	12.3	19.09	2.793
6	6.03	385	602	325.2	3.94	161.6	14.1	15.41	1.051
7	6.37	496	546	50.7	3.62	131.5	107.5	1.23	5.417
8	6.68	495	552	27.8	3.33	133.7	118.7	1.13	2.125
9	7.00	488	544	23.2	3.22	125.6	115.3	1.13	1.612
10	7.31	484	540	19.7	3.13	119.5	113.0	1.13	1.361
11	7.62	483	539	17.2	3.05	116.3	112.8	1.15	1.236
12	7.94	483	540	15.6	2.99	114.1	112.7	1.19	1.182
13	8.25	484	541	14.4	2.95	111.6	111.9	1.25	1.154
14	8.56	484	540	13.6	2.91	108.4	110.0	1.32	1.127
15	8.87	483	538	13.1	2.88	104.6	107.1	1.40	1.092
16	9.18	482	536	12.8	2.86	100.4	103.6	1.47	1.047
17	9.49	481	533	12.6	2.85	96.2	99.9	1.55	0.995
18	9.80	480	530	12.3	2.83	92.1	96.3	1.60	0.936
19	10.11	479	528	12.0	2.80	88.3	93.2	1.62	0.866
20	10.41	476	523	11.3	2.75	84.5	91.0	1.58	0.769

Table 1b Variation of shock parameters for RB and FB

day	AU	u_1 km/s	S km/s	p_2^*/p_1^*	n_2/n_1	$\lvert u_1-u_2\rvert$ km/s	C_{f1} km/s	M_1	β_1
				REVERSE SHOCK RB					
0	4.93	405	347	3.1	1.77	25.0	35.8	1.19	0.461
1	5.13	402	349	3.4	1.83	23.7	31.5	0.99	0.406
2	5.33	398	350	3.7	1.90	23.0	27.9	0.73	0.392
3	5.54	395	350	4.1	1.98	22.5	25.0	0.16	0.396
4	5.74	393	349	4.6	2.07	22.3	22.7	0.80	0.413
5	5.94	391	349	5.1	2.16	22.3	20.7	1.07	0.439
6	6.14	389	349	5.7	2.26	22.4	19.0	1.20	0.474
7	6.35	496	390	1.8	1.41	43.3	132.6	0.80	25.141
8	6.57	490	388	1.8	1.42	42.6	127.4	0.80	53.647
9	6.80	487	408	2.0	1.49	39.1	102.2	0.77	7.191
10	7.04	485	421	2.3	1.56	36.5	86.8	0.75	1.675
11	7.29	484	427	2.5	1.62	35.1	78.5	0.73	0.777
12	7.53	481	427	2.7	1.66	35.5	75.5	0.71	0.497
13	7.78	475	422	2.9	1.69	37.2	76.6	0.70	0.365
14	8.02	469	413	3.0	1.71	39.9	80.4	0.70	0.290
15	8.26	461	402	3.0	1.73	43.0	85.6	0.69	0.246
16	8.48	453	390	3.1	1.74	46.2	91.1	0.69	0.223
17	8.71	445	380	3.2	1.75	49.0	95.2	0.68	0.219
18	8.92	439	373	3.3	1.78	50.8	96.3	0.68	0.233
19	9.14	433	370	3.4	1.81	51.4	94.3	0.67	0.262
20	9.35	429	369	3.6	1.85	50.9	90.2	0.66	0.304
				FORWARD SHOCK FB					
0	6.20	370	537	6.1	2.25	93.0	77.8	2.06	0.015
1	6.51	376	523	7.8	2.43	86.3	61.1	3.09	0.027
2	6.80	374	505	12.3	2.80	84.1	43.8	5.02	0.098
3	7.09	367	492	19.4	3.14	84.8	33.2	7.62	0.318
4	7.37	361	483	24.0	3.30	85.1	29.1	9.24	0.642
5	7.65	356	476	21.5	3.24	83.2	30.2	8.69	0.632
6	7.92	350	471	16.0	3.02	81.0	35.4	7.11	0.359
7	8.20	348	473	12.4	2.82	80.8	41.5	1.01	0.178
8	8.47	348	479	10.4	2.68	81.7	47.2	0.84	0.091
9	8.75	349	483	9.1	2.56	81.2	51.6	1.13	0.054
10	9.03	351	484	8.2	2.48	79.3	54.1	1.29	0.040
11	9.31	352	483	7.5	2.41	76.6	55.5	1.35	0.035
12	9.59	354	482	7.0	2.35	73.8	56.3	1.30	0.033
13	9.87	355	481	6.5	2.30	71.2	56.9	1.17	0.031
14	10.14	356	480	6.1	2.25	68.8	57.5	0.98	0.030
15	10.42	357	479	5.8	2.21	66.6	58.0	0.77	0.029
16	10.70	358	478	5.5	2.17	64.7	58.4	0.55	0.028
17	10.97	359	477	5.3	2.14	63.1	58.7	0.36	0.027
18	11.25	359	477	5.2	2.11	61.7	58.9	0.23	0.026
19	11.53	360	476	5.0	2.09	60.6	59.1	0.17	0.025
20	11.80	360	475	4.9	2.07	59.6	59.2	0.16	0.024

FIGURE CAPTIONS

Figure 1. The initial conditions for this study are generated from the two pressure waves A and B bounded by shock pairs observed by Voyager 2 in October 1978. The total pressure, magnetic field and plasma density in the shock compression region are significantly greater than those outside its shock boundaries.

Figure 2. The two shock pairs (A and B) have been observed by both Voyager 1 and 2 . As Voyager 2 data are used as input, the initial state of the four shocks (shock speeds and shock strengths) have to be carefully adjusted so that the plasma and field calculated at the Voyager 1 orbit are in good agreement with observation.

Figure 3. The coalescence of two pressure waves produced a second-generation shock compression region. A contact surface (CS) appeared in the new compression region.

Figure 4. The variation of the state of the four shock waves (represented by two parameters the shock speed and the density ratio) during the 20 days period and their sudden changes due to collision on day 6.8.

Figure 5. After collision, the flow speed remained continuous across the contact surface in the second-generation shock compression region. As FA moved into a region with increasing flow speed and RB moved into a region with decreasing flow speed, the velocity profile evolved into a sawtooth configuration on day 20.

Figure 6. Two distinct pressure waves are seen on day 0 at the bottom panel. After the collision of FA and RB, the profile of the total pressure changed significantly. The total pressure in the second-generation shock compression region is two orders of magnitude greater than that predicted by an adiabatic solar wind under the assumption that there were no shocks in the heliosphere.

Figure 7. The temperature is discontinuous across a contact surface that has formed as a result of the collision between FA and RB. Because the two shock pairs are not equal in shock strength, in the second-generation shock compression region the temperature is higher on the side of the stronger initial shock pair.

Figure 8. The number density is also discontinuous across the contact surface. In the second-generation shock compression region the plasma density is lower on the side of the stronger initial shock pair.

Figure 9. The balance of the total pressure across CS requires that the magnetic pressure must be lower on the side of CS with higher temperature.

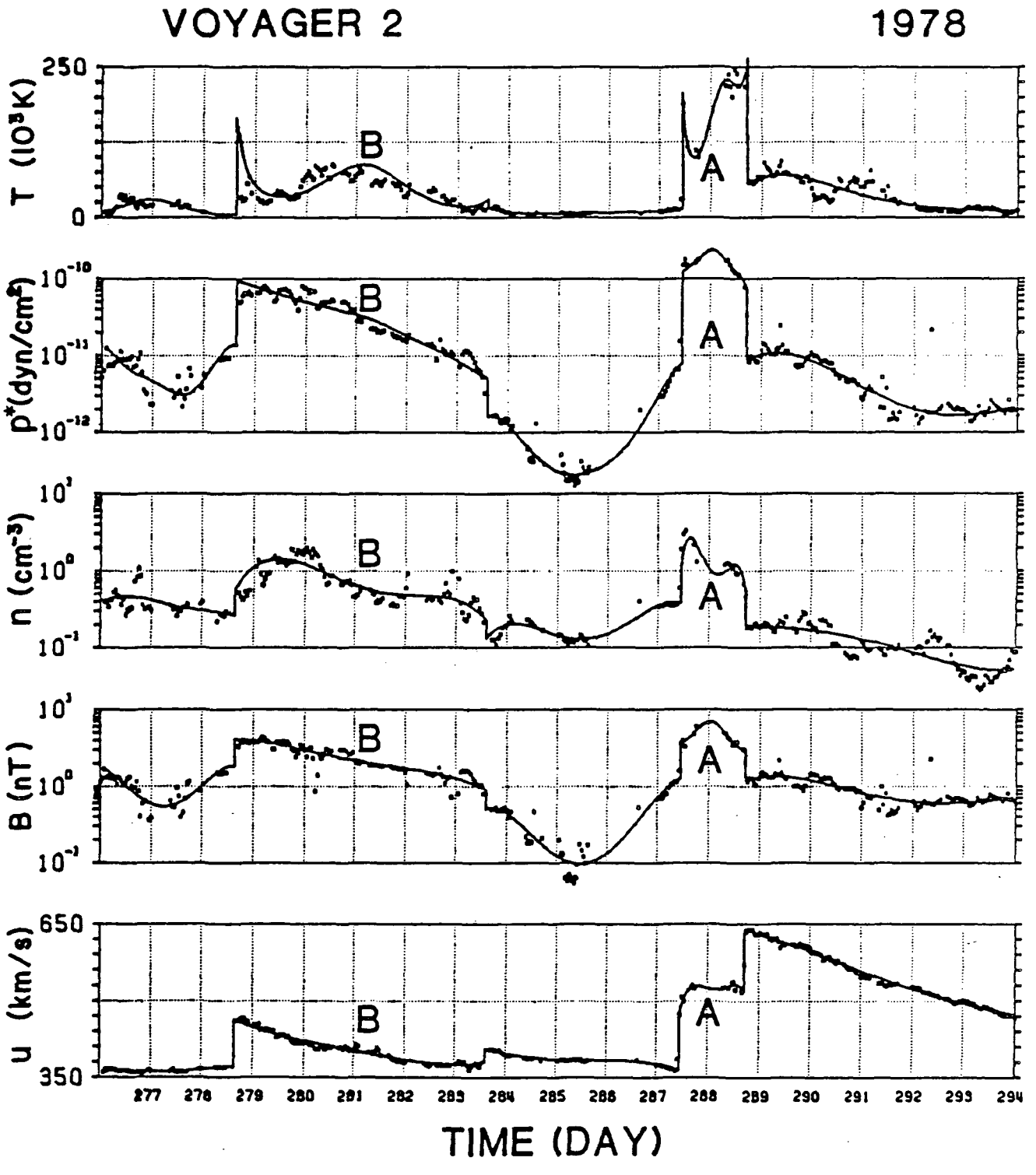

Figure 1. The initial conditions for this study are generated from the two pressure waves A and B bounded by shock pairs observed by Voyager 2 in October 1978. The total pressure, magnetic field and plasma density in the shock compression region are significantly greater than those outside its shock boundaries.

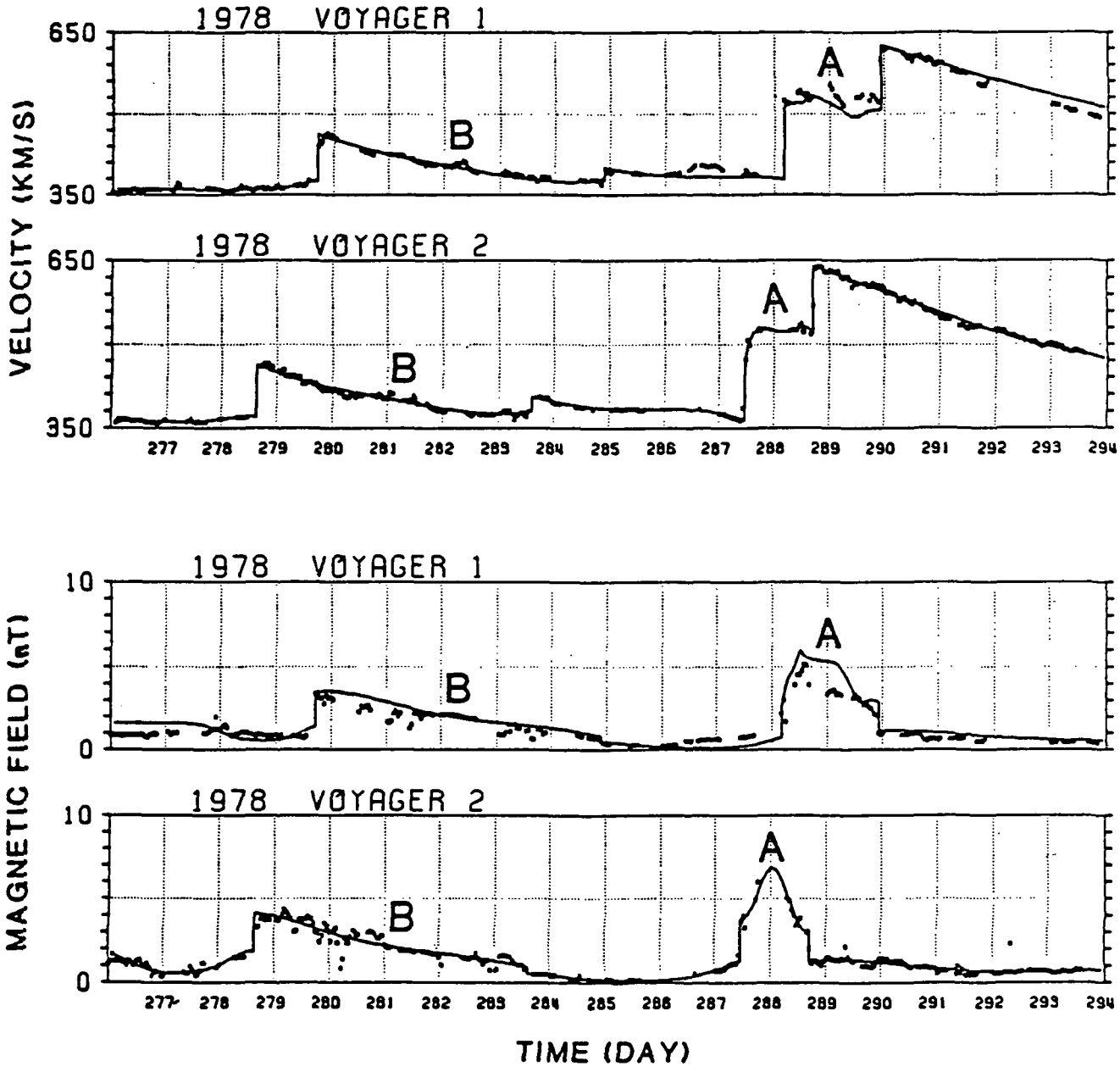

Figure 2. The two shock pairs (A and B) have been observed by both Voyager 1 and 2 . As Voyager 2 data are used as input, the initial state of the four shocks (shock speeds and shock strengths) have to be carefully adjusted so that the plasma and field calculated at the Voyager 1 orbit are in good agreement with observation.

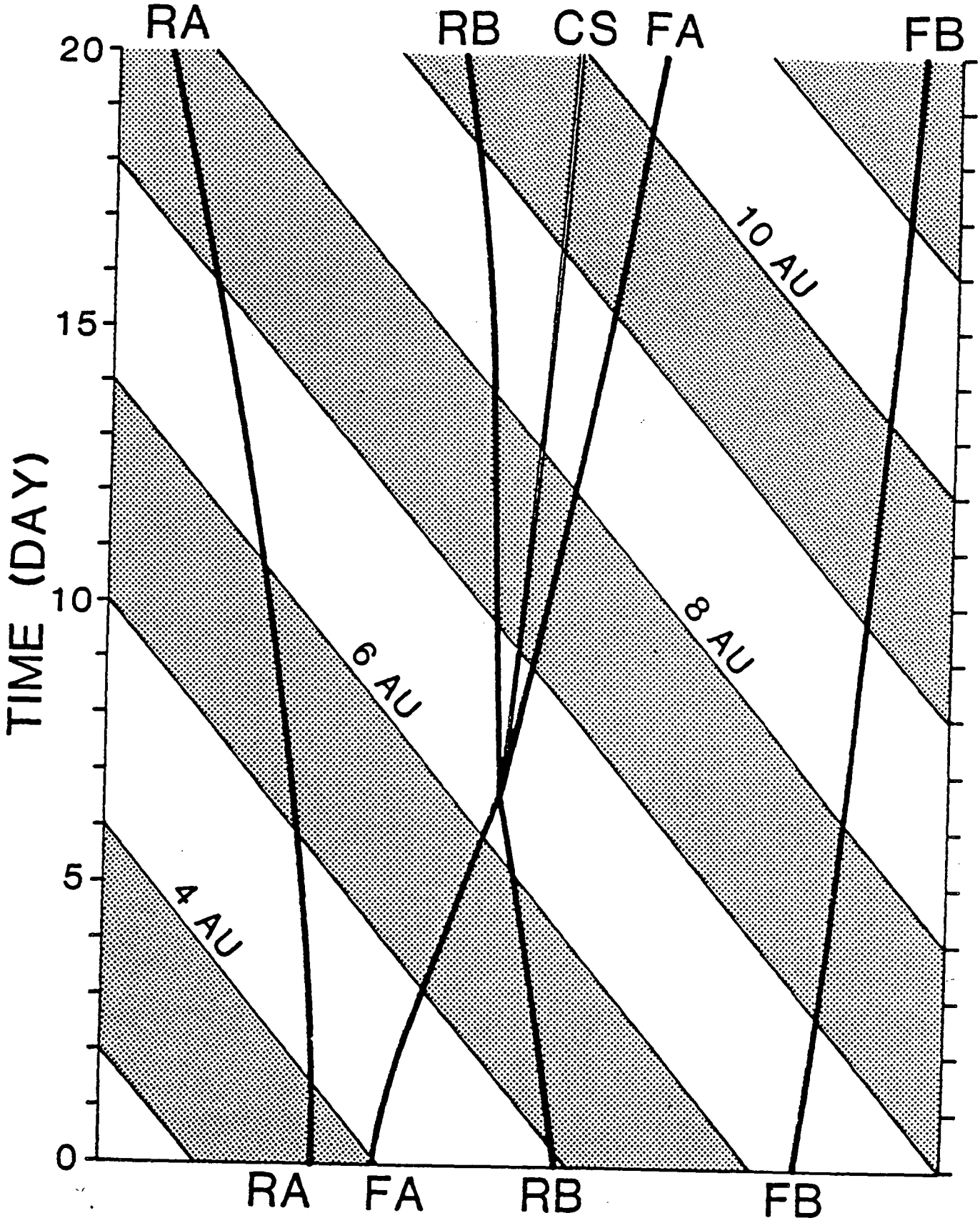

Figure 3. The coalescence of two pressure waves produced a second-generation shock compression region. A contact surface (CS) appeared in the new compression region.

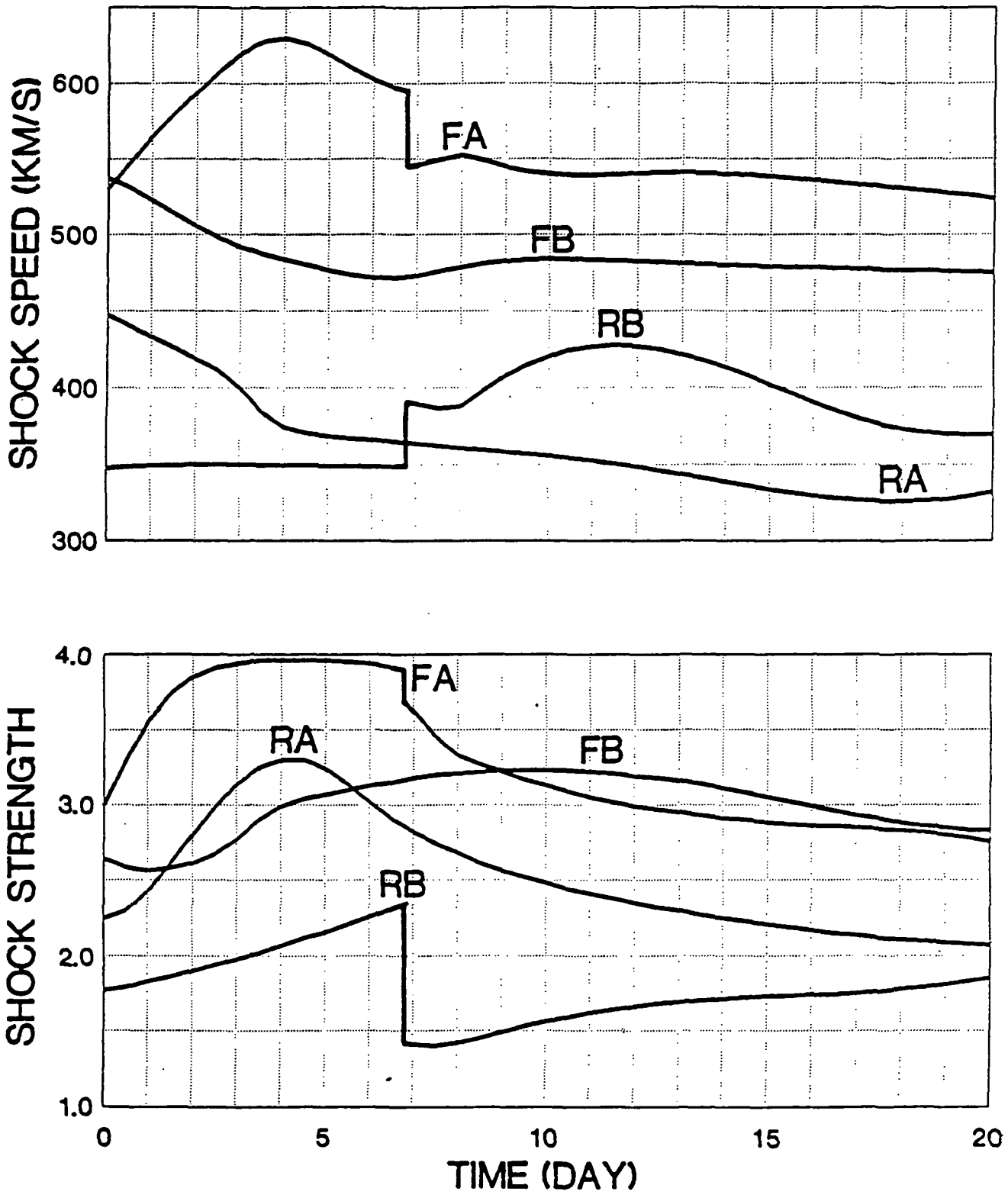

Figure 4. The variation of the state of the four shock waves (represented by two parameters the shock speed and the density ratio) during the 20 days period and their sudden changes due to collision on day 6.8.

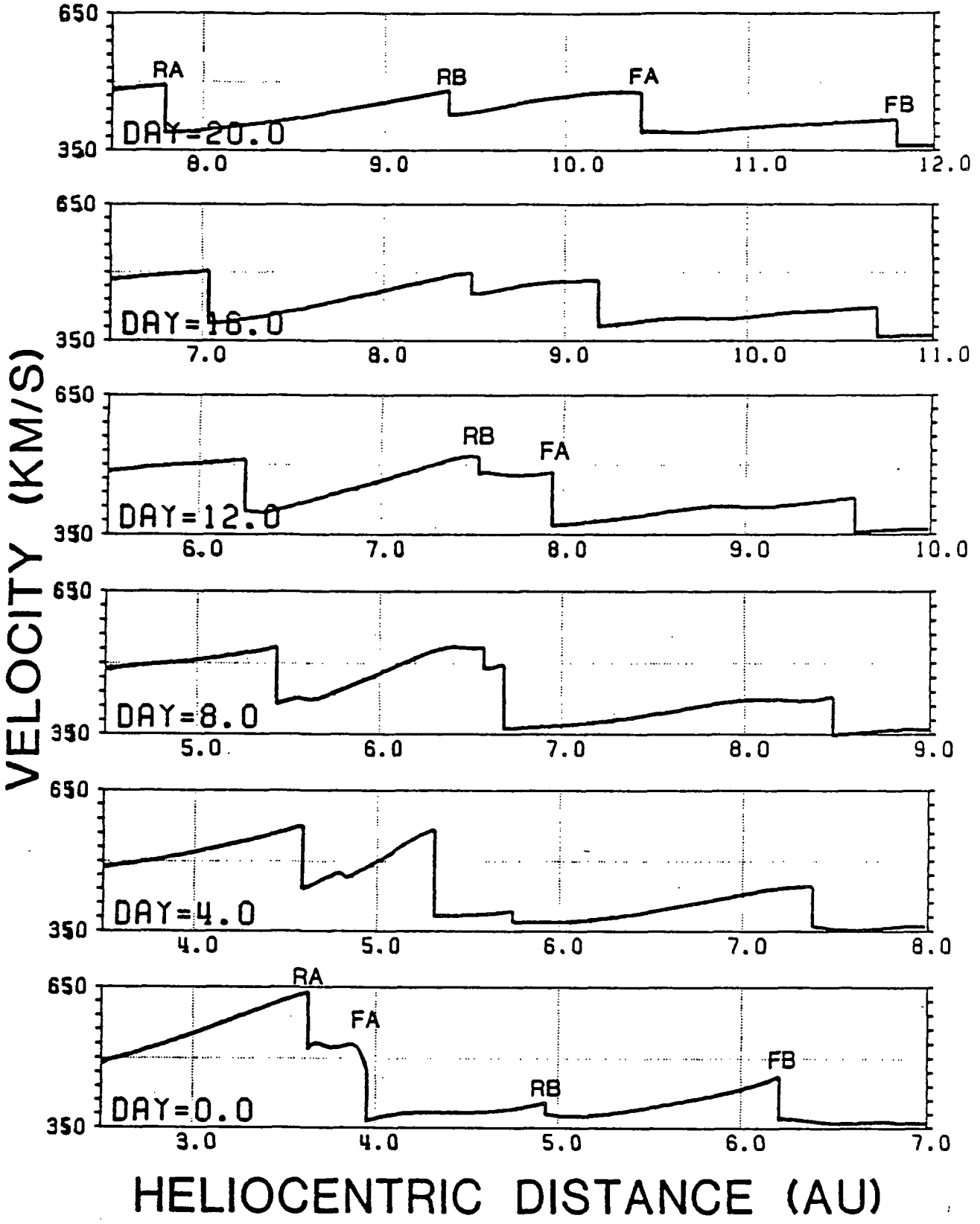

Figure 5. After collision, the flow speed remained continuous across the contact surface in the second-generation shock compression region. As FA moved into a region with increasing flow speed and RB moved into a region with decreasing flow speed, the velocity profile evolved into a sawtooth configuration on day 20.

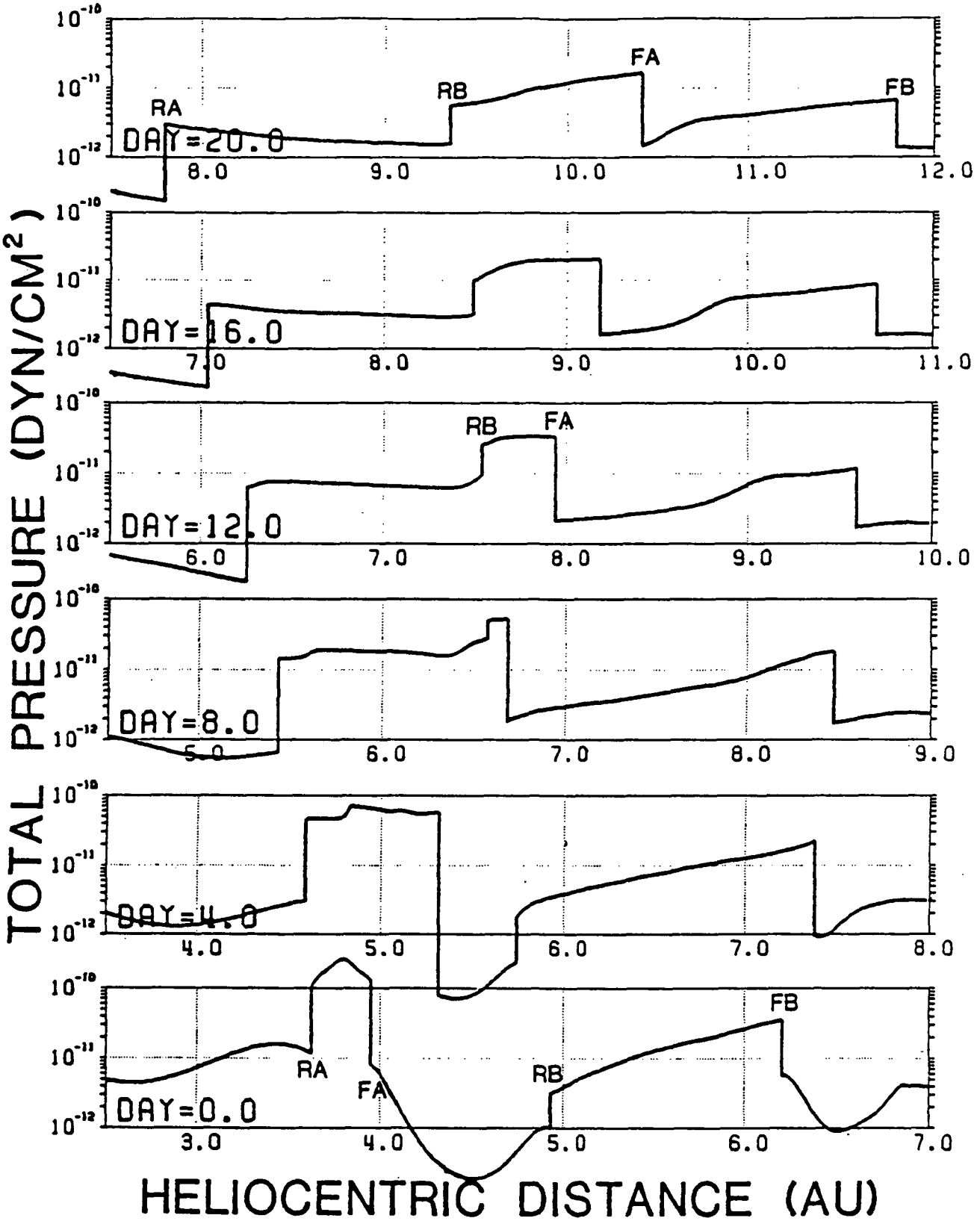

Figure 6. Two distinct pressure waves are seen on day 0 at the bottom panel. After the collision of FA and RB, the profile of the total pressure changed significantly. The total pressure in the second-generation shock compression region is two orders of magnitude greater than that predicted by an adiabatic solar wind under the assumption that there were no shocks in the heliosphere.

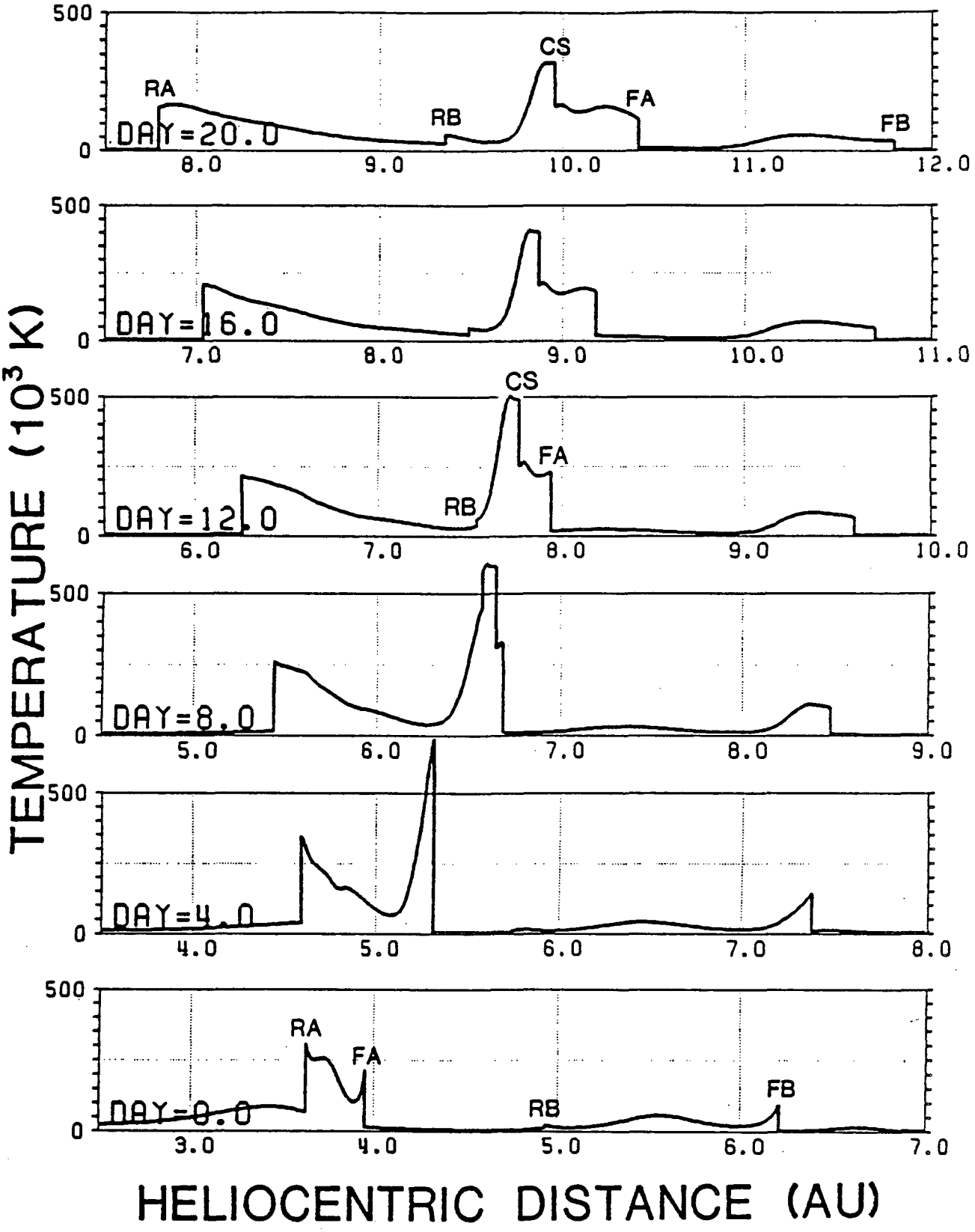

Figure 7. The temperature is discontinuous across a contact surface that has formed as a result of the collision between FA and RB. Because the two shock pairs are not equal in shock strength, in the second-generation shock compression region the temperature is higher on the side of the stronger initial shock pair.

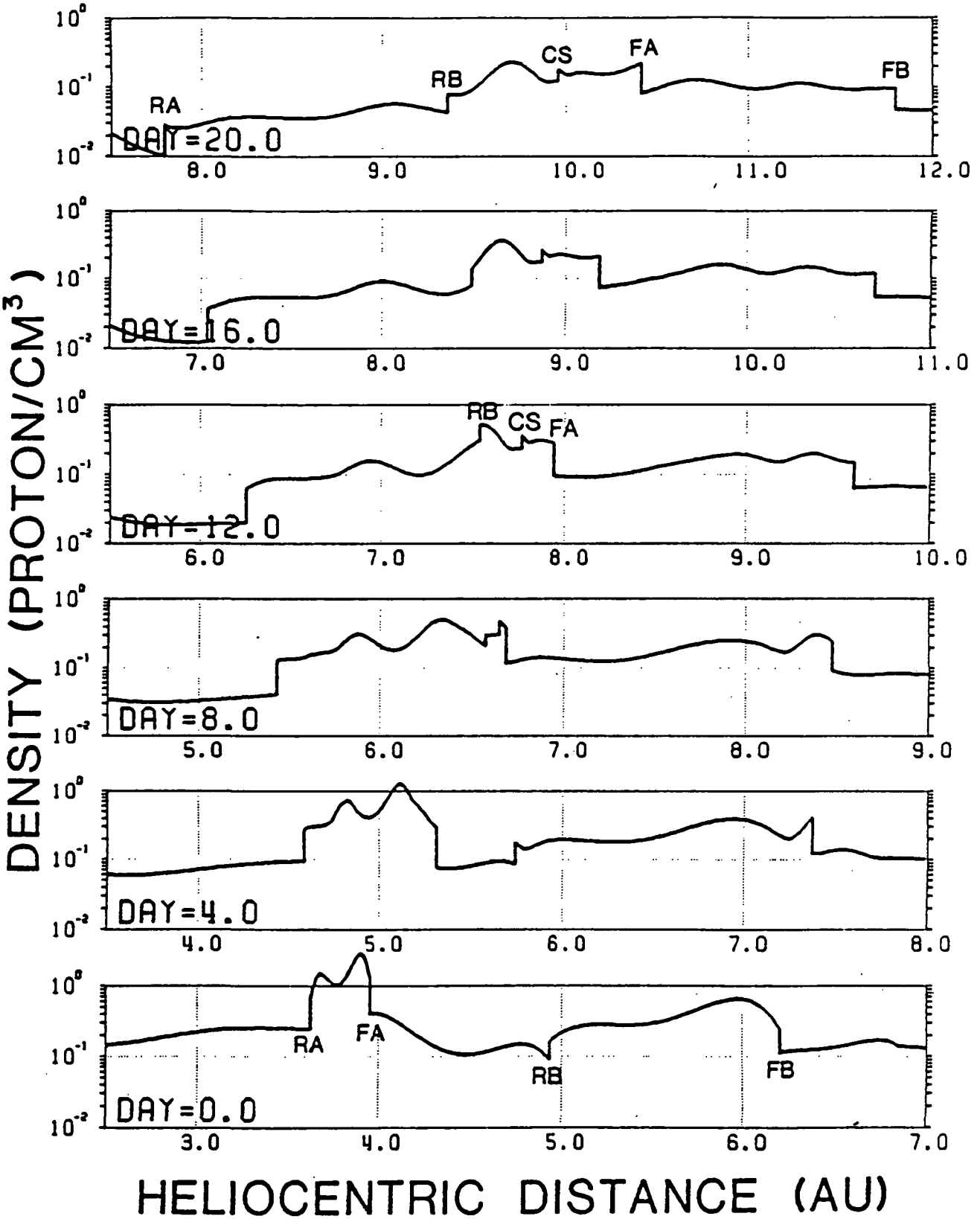

Figure 8. The number density is also discontinuous across the contact surface. In the second-generation shock compression region the plasma density is lower on the side of the stronger initial shock pair.

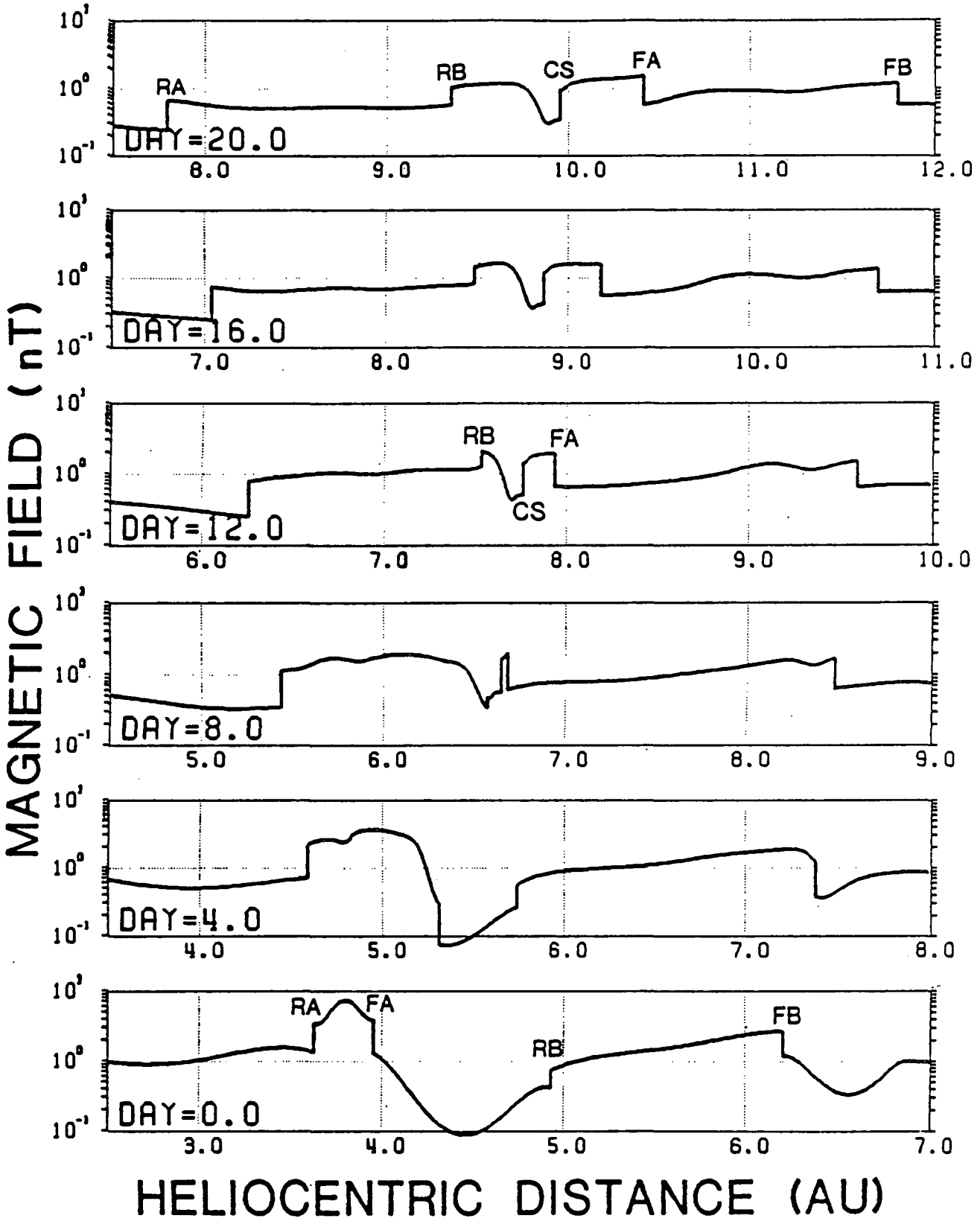

Figure 9. The balance of the total pressure across CS requires that the magnetic pressure must be lower on the side of CS with higher temperature.

BIBLIOGRAPHIC DATA SHEET

1. Report No.	2. Government Accession No.	3. Recipient's Catalog No.
TM 86120		

4. Title and Subtitle	5. Report Date
Coalescence of Two Pressure Waves Associated with Stream Interactions	April 1984
	6. Performing Organization Code

7. Author(s)	8. Performing Organization Report No.
Y. C. Whang and L. F. Burlaga	

9. Performing Organization Name and Address	10. Work Unit No.
NASA/GSFC Laboratory for Extraterrestrial Physics Interplanetary Physics Branch, Code 692 Greenbelt, MD 20771	11. Contract or Grant No.
	13. Type of Report and Period Covered Technical Memorandum
12. Sponsoring Agency Name and Address	14. Sponsoring Agency Code

15. Supplementary Notes

16. Abstract An MHD unsteady 1-D model is used to simulate the interaction and coalescence of two pressure waves in the outer heliosphere. Each of the two pressure waves was a compression region bounded by a shock pair. Computer simulation using Voyager data as input demonstrates the interaction and coalescence process involving one pressure wave associated with a fast stream and the other pressure wave without a fast stream. The process produced a significant change in the magnetic field and plasma signatures. The propagation of the forward and reverse shocks first widened the radial dimension of the shock compression region with increasing heliocentric distances. The shocks belonging to two neighboring compression regions eventually collided and the two compression regions began to overlap with each other. Both shocks continued to propagate after the collision but they were weakened. As a result of the collision, a contact surface formed in the second generation compression region bounded by the two shocks. The second shock compression further enhanced the magnetic field, plasma density and temperature in the new compression region. This type of interaction is a dominant dynamical process in the outer heliosphere, and it can significantly and irreversibly alter the structure of the medium.

17. Key Words (Selected by Author(s))	18. Distribution Statement
Shocks, solar wind, interplanetary magnetic field	

19. Security Classif. (of this report)	20. Security Classif. (of this page)	21. No. of Pages	22. Price*
U	U	33	

*For sale by the National Technical Information Service, Springfield, Virginia 22161